Journal of the European Ceramic Society **18** (1998) 51–57

PII: S0955-2219(97)00106-4
0955-2219/98/$19.00 + 0.00

Mechanical Behavior and Microstructure of SiC and SiC/TiB_2 Ceramics

Dong-Hau Kuo† and Waltraud M. Kriven*

Department of Materials Science and Engineering, University of Illinois at Urbana-Champaign, Urbana, IL 61801, USA

(Received 14 February 1997; accepted 30 May 1997)

Abstract

Toughness characteristics and associated microstructural behavior in two kinds of SiC and TiB_2 particulate-reinforced SiC composites were studied. From indentation- strength tests, the Al_2O_3-doped, high volume fraction β-SiC/TiB_2 showed a distinctive flaw tolerance and a higher retained strength in the long-crack region, as compared with β-SiC alone. On the other hand, the boron- and carbon-doped, low volume fraction, α-SiC/TiB_2 exhibited a higher retained strength without an apparent improvement in flaw tolerance, as compared with α-SiC. Crack bridging and sliding and pullout of TiB_2 particulates toughened the β-SiC/TiB_2, while only crack bridging by TiB_2 occurred in α-SiC/TiB_2 with difficulty in grain sliding and pullout. A quantitative evaluation of the indentation-strength data revealed a sharp rising toughness curve for β-SiC/TiB_2. The enhanced long-crack toughness originated from the weak interface created by the TiB_2 and sintering additives. © *1997 Elsevier Science Limited.*

1 Introduction

Silicon carbide (SiC) is one of the important structural ceramics for high temperature applications because of its excellent mechanical properties. However, its low fracture toughness and the high flaw sensitivity limit its widespread applications.

It has been demonstrated that the fracture toughness and the flaw tolerance of ceramics can be improved by controlling the microstructure and by incorporating second phases (particulates, whiskers). By in-situ forming of elongated-shaped reinforcements, significant improvements in flaw tolerance and toughening have been achieved in silicon nitride.[1,2] Different sintering additives have been used to densify SiC and to modify its microstructure. The liquid-phase-sintered SiC densified with Al_2O_3 and Y_2O_3 as sintering additives exhibits a fracture toughness as high as 7 MPa·$m^{1/2}$ [3–5]. SiC also has been reinforced by TiC [6,7] and TiB_2 [8–12] particles as a dispersed phase to improve fracture toughness. The SiC/TiB_2, composite has shown a low electrical resistivity (< 1 Ω·cm), which makes it a good electrical conductor and has good electrical-discharge machinability.[8] The flexural strength, fracture toughness, and toughness-curve (R- or T-curve) of pressureless sintered SiC composites reinforced with TiB_2 have been measured.[8–12] Toughening mechanisms such as crack deflection, crack bridging, and microcracking have been proposed for this material. As a major candidate for armor ceramics, the retained strength (post-damage strength) of the SiC/TiB_2 composite is an important indicator of the performance of armors.[13] However, the retained strength behavior of SiC/TiB_2 has not yet been discussed.

In the present study, indentation-strength tests were used to determine the retained strength (post-indented strength), flaw tolerance, and toughness-curve characteristics of two kinds of SiC and SiC/TiB_2 composites. β-SiC and, β-SiC/TiB_2 composites which were hot pressed with an AlO_3 sintering aid, were compared with the well-studied α-SiC and α-SiC/TiB_2 composites, which were sintered with boron and carbon additives. The effects of microstructural changes resulting from the sintering additives, as well as from TiB_2 content on the toughening behavior and flaw tolerance for these materials have been investigated.

2 Experimental Procedure

Four materials of SiC and its composites reinforced with TiB_2 were investigated. A commercial α-SiC (Hexoloy SA) and a 15 vol% TiB_2/α-SiC composite (α-SiC/TiB_2, Hexoloy ST) were obtained from the Carborundum company, Niagara Falls, NY.

*To whom correspondence should be addressed.
†Present address: Institut of Materials Science and Engineering, National Dong Hwa University, Shoufeng, Hualien, Taiwan.

They were sintered at temperatures above 2000°C using boron and carbon as sintering aids in an inert atmosphere.[8] They had 3–8-μm grain sizes for SiC and 1–5-μm particle sizes for the discrete TiB_2 particles. A β-SiC and a 30-vol% TiB_2/β-SiC composite (β-SiC/TiB_2) were supplied by the Alcoa company, Alcoa Center, PA. They were hot-pressed at 1950°C under 18 MPa in an argon atmosphere for 2 h, using Al_2O_3 as a sintering aid. β-SiC single phase material had a grain size ranging from 0·8 to 3 μm. The TiB_2 particles, with particle sizes ranging from 3 to 8 μm in the β-SiC matrix, were not fully discrete, but tended to be adjacent to other TiB_2 particles.

Mechanical testing was carried out on rectangular beams using the indentation-strength method. Because of the confirmation of stable crack growth of SiC/TiB_2 by Gu and Faber[10] using the double cantilever beam technique and the confirmation of indentation parameters of and χ on SiC by Padture and Lawn,[14] this test technique can be applied to measure T curve with confidence. Specimens had dimensions of 25 × 2·5 (width) × 2·2 (depth) mm. Specimen surfaces were polished down to a 1-μm diamond paste finish and the edges of the tensile surfaces were bevelled with a 3-μm diamond paste. Specimens for flexural tests were indented in air at the center of tensile surfaces, with a Vickers diamond pyramid, at constant loads from $P=2$ to 300 N. Some flexual bars were left without Vickers indentations, for measurement of 4-pt flexural strengths.

The rectangular bars were tested in a four-point bend fixture (20 mm outer span and 10 mm inner span) mounted on a universal testing machine (Model 4502, Instron, Canton, MA). To lessen environmental effects, a drop of silicone oil was placed on the indented site, and the bar was broken in rapid loading (failure time < 10 ms). If the flexural failures of the bars did not originate from the indentations, these calculated strengths were included in the 4-pt flexural strengths. Average strength values with one standard deviation from four or five successful tests, were measured as a function of indentation load.

To construct the toughness curve, the Vickers hardness was obtained by the indentation technique. Young's modulus was obtained by the pulse echo, ultrasonic technique (NDT-150, Nortec Inc., Kennewick, WA). Fracture behavior was analyzed by scanning electron microscopy (SEM, Model DS-130, International Scientific Instruments, Santa Clara, CA). Transmission electron microscopy (TEM, Model CM-12, Philips Instruments, Inc., Mahwah, NJ) and energy dispersive spectroscopy (EDS, Model EDAX-9900, EDAX International, Prairie View, IL) were used to characterize the microstructure and microchemistry, respectively.

3 Results

3.1 Observation of crack–microstructure interactions

SEM crack propagation profiles of radial cracks by Vickers indentation tests on SiC are shown in Fig. 1. In the boron- and carbon-doped α-SiC,

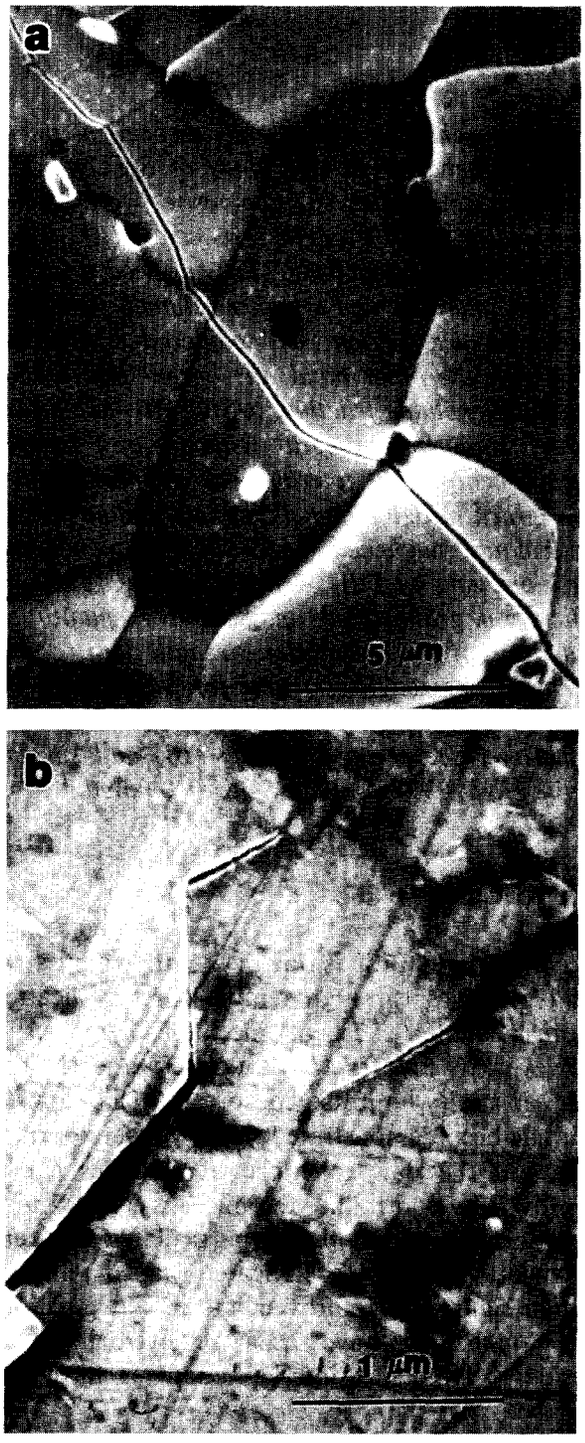

Fig. 1. (a) Transgranularly fractured boron- and carbon-doped α-SiC and (b) intergranularly fractured Al_2O_3-doped β-SiC showing crack bridging after Vickers indentation.

transgranular fracture occurred, as seen in Fig. 1(a). However, intergranular fracture was observed in Al doped β-SiC. Crack bridging by grains located at the radial crack tips was observed in SiC, as seen in Fig. 1(b).

In the composites, cracks usually deflected around or were bridged by TiB_2 particles. A typical crack bridging by a TiB_2 particle in α- and β-SiC/TiB_2 near a radial crack tip was evidenced in Fig. 2(a) and (b), respectively. Although the bridged TiB_2 posed a crack closure force to toughen these composites, the TiB_2 in the α-SiC/TiB_2 had much difficulty in sliding and pullout. Instead a crack [arrowed in Fig. 2(a)] initiated at the debond crack as the applied load increased.

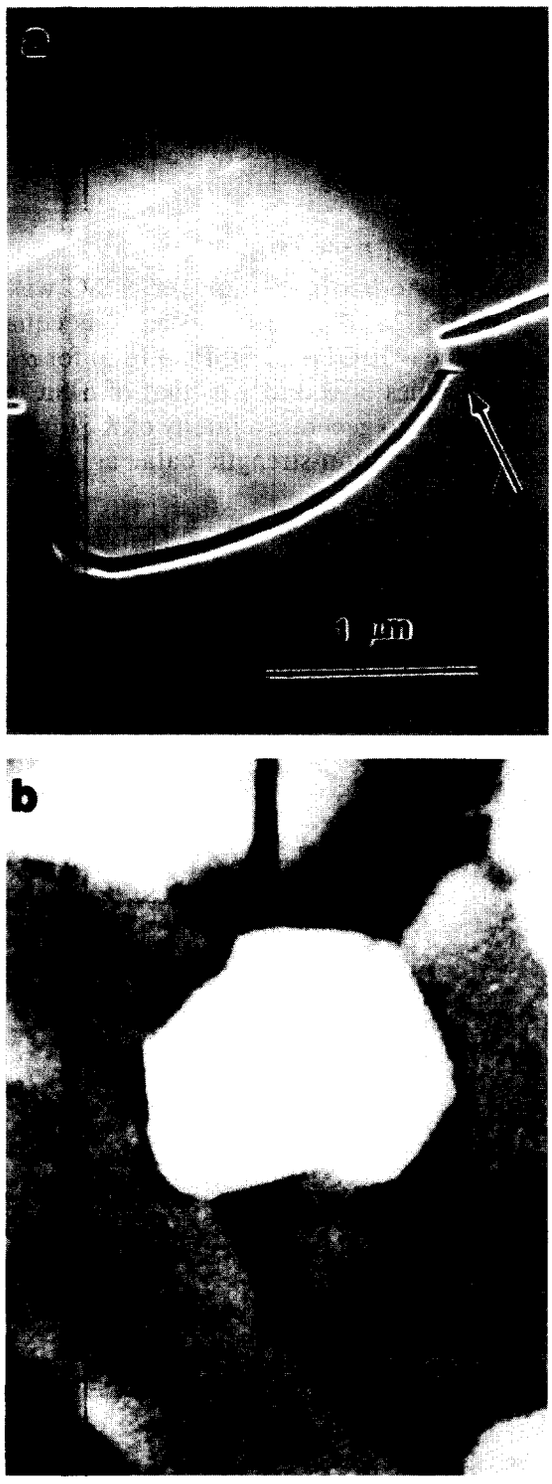

Fig. 2. Bridging behavior of a TiB_2 particle in (a) α-SiC/TiB_2 and β-SiC/TiB_2. The arrow in (a) indicates the evidence of crack bridging behavior.

3.2 Indentation-strength and toughness curves

Results of the indentation load (P)-strength (σ_F) testing are presented in Fig. 3 for α-SiC and α-SiC/TiB_2, and in Fig. 4 for β-SiC and β-SiC/TiB_2. As shown in Figs 3 and 4, the fracture strengths of unindented α-SiC, α-SiC/TiB_2, β-SiC. and β-SiC/TiB_2 were 458 ± 35, 465 ± 39, 394 ± 32, and 327 ± 40 MPa, respectively. The fracture strengths of α-SiC and α-SiC/TiB_2 were close to each other. The slope for α-SiC was close to $-1/3$, which indicated a single-valued toughness. The $\sigma_F(P)$ response of α-SiC/TiB_2 deviated slightly from the $P^{-1/3}$ dependence, which was expected to have a

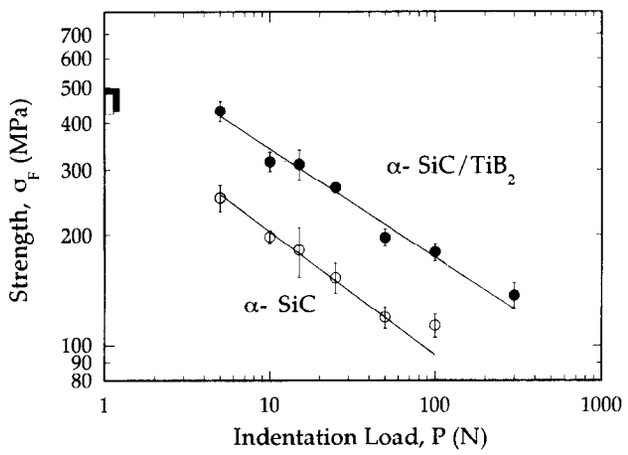

Fig. 3. Indentation-strength data for α-SiC and α-SiC/TiB_2. Boxes on the left axis are strengths representing data from unindented specimens. The line passing through α-SiC data is the line of best fit for the condition $\sigma_F \mu P^{-1/3}$. The line for α-SiC/TiB_2 is the linear least-squares fit to the data.

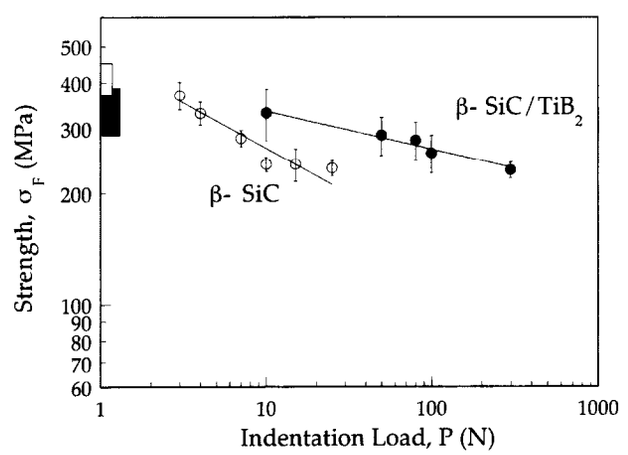

Fig. 4. Indentation-strength data for β-SiC and β-SiC/TiB_2. Boxes on the left axis are strengths representing data from unindented specimens. The lines are the linear least-squares fit to the data.

slightly rising toughness curve $T(c)$. The main effect of TiB_2 in the α-SiC/TiB_2 was to increase the retained strength (post-indentation strength) of SiC, rather than on flaw tolerance (relative to the slope of the $\sigma_F(P)$ response). On the other hand, the fracture strength of β-SiC decreased as 30 vol% TiB_2 was added. Both β-SiC and SiC/TiB_2, exhibited flaw tolerance, especially β-SiC/TiB_2, which showed a strongly enhanced long-crack strength (Fig. 4). The significant flaw tolerance of β-SiC/TiB_2 corresponds to the near-flat slope of the $\sigma_F(P)$ response. The effect of TiB_2 in β-SiC/TiB_2 was to increase the retained strength at the long-crack region and to enhance the flaw tolerance.

Toughness curves $T(c)$ can be deconvoluted from the data in Figs 3 and 4 in accordance with an indentation-strength K-field analysis suggested by Mai and Lawn[15] and Lawn.[16] Under the action of an applied stress σ_A, radial cracks of size c produced at an indentation load P extend according to the equilibrium condition[15]

$$K_A'(c) = \psi\sigma_A c^{1/2} + \chi P/c^{3/2} = T(c) \qquad (1)$$

where $K_A'(c)$ is an effective applied stress intensity factor and $T(c)$ defines the toughness curve for the material; ψ is a geometrical coefficient that characterizes the crack configuration;[17] and $\chi \propto (E/H)^{1/2}$ is a residual-contact coefficient.[17,18] For a given load P, failure occurs at that applied stress $\sigma_A = \sigma_F$, which corresponds to a 'tangency condition'

$$dK_A'(c)/dc = dT(c)/dc \qquad (2)$$

Accordingly, if the coefficients ψ and χ can be properly calibrated, families of curves can be generated from the data in Figs 3 and 4. Toughness curves $T(c)$ should be determined as envelopes to these families of curves.[19] Such constructions for SiC and SiC/TiB_2 are made below.

3.2.1. α-SiC and α-SiC/TiB_2

The construction of a toughness curve for α-SiC has been demonstrated by Padture and Lawn,[14] by assuming that material-independent $\psi = 0{\cdot}77$ and $\chi = 0{\cdot}067$, after calibration with the well studied Al_2O_3. In this study, these parameters were followed, except for the χ value of α-SiC/TiB_2. According to the relationship of $\chi \propto (E/H)^{1/2}$, the modulus-to-hardness ratio for α-SiC/TiB_2 was (E/H) = (420 GPa/29·7 GPa) = 14·1 and χ was calibrated to be 0·062. As the $\sigma_F(P)$ response followed the $P^{-1/3}$ dependence, α-SiC had a toughness, $T(c) = T_0 =$ constant. By solving eqns (1) and (2) with $T = T_0$ at the condition of crack growth instability ($d\sigma_A/dc = 0$), we can obtain[19]

$$\sigma_A = \sigma_F = (3T_0/4\psi)(T_0/4\chi P)^{1/3} \qquad (3)$$

From the data in Fig. 3, the T_0 value can be obtained for the known brittle α-SiC by curve-fitting the data to eqn (3). The best-fit line in Fig. 3 for α-SiC corresponds to the condition under $T_0 = 2{\cdot}2\ \text{MPa}\cdot\text{m}^{1/2}$. Families of $K_A'(c)$ curves can be generated from the indentation-strength data in Fig. 3 and eqn (1) for α-SiC [Fig. 5(a)] and α-SiC/TiB_2 [Fig. 5(b)], respectively. It was apparent that the envelope of tangency points was approximately horizontal for α-SiC, while it slightly increased for α-SiC/TiB_2. The horizontal envelope indicated a single-valued toughness for α-SiC. The slightly increased envelope for α-SiC/TiB_2 suggested a limited toughening effect.

3.2.2. β-SiC and β-SiC/TiB_2

The modulus-to-hardness ratio for β-SiC was (E/H) = (430 GPa/26 GPa) = 16·5, which was equal to an E/H value (410 GPa/24·5 GPa = 16·5) for α-SiC. The same values of ψ and χ as that of α-SiC were used for β-SiC to generate a family of $K_A'(c)$ curves from the indentation-strength data, as shown in

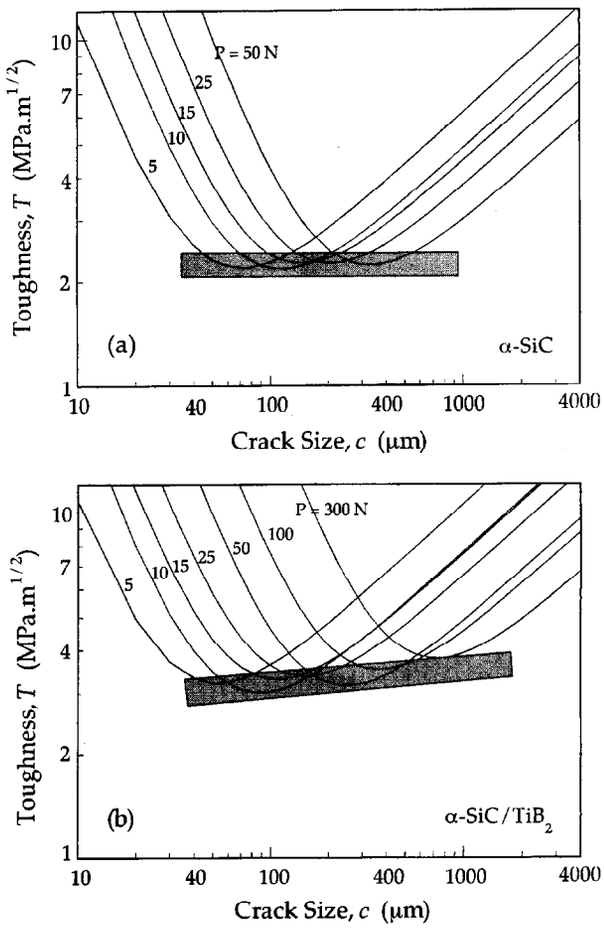

Fig. 5. Toughness-curve diagrams for (a) α-SiC and (b) α-SiC/TiB_2. The family of solid curves are plots of $K_A'(c)$ in eqn (1), using strength data from Fig. 3. Shaded bands are T-curves, plotted as locus of tangency points to $K_A'(c)$ curves.

Fig. 6(a). The modulus-to-hardness ratio for β-SiC/TiB_2 was (E/H) = (430 GPa/33·6 GPa) = 12·8. The χ value was modified to be 0·059 for β-SiC/TiB_2. A family of $K_A'(c)$ curves generated from the indentation-strength data in Fig. 4 is shown in Fig. 6(b) for β-SiC/TiB_2. We observed that the envelope of tangency points only slightly increased for α-SiC, while yielding a rising $T(c)$ curve for β-SiC/TiB_2. In the long crack region, the toughness of β-SiC/TiB_2 increased relative to the β-SiC by a factor of ~3.

4 Discussion

Boron and carbon for sintering the α-type materials formed granules at grain boundaries (Fig. 7). The transgranular fracture occurring in α-SiC [Fig. 1(a)] indicated strong bonding between SiC grains. A slightly rising $T(c)$ curve for α-SiC/TiB_2 arose mainly from the TiB_2 contribution. As seen in Fig. 2(a), the crack was bridged by a TiB_2 particle. The T-curve behavior was due mainly to crack bridging in non-transformable, non-cubic

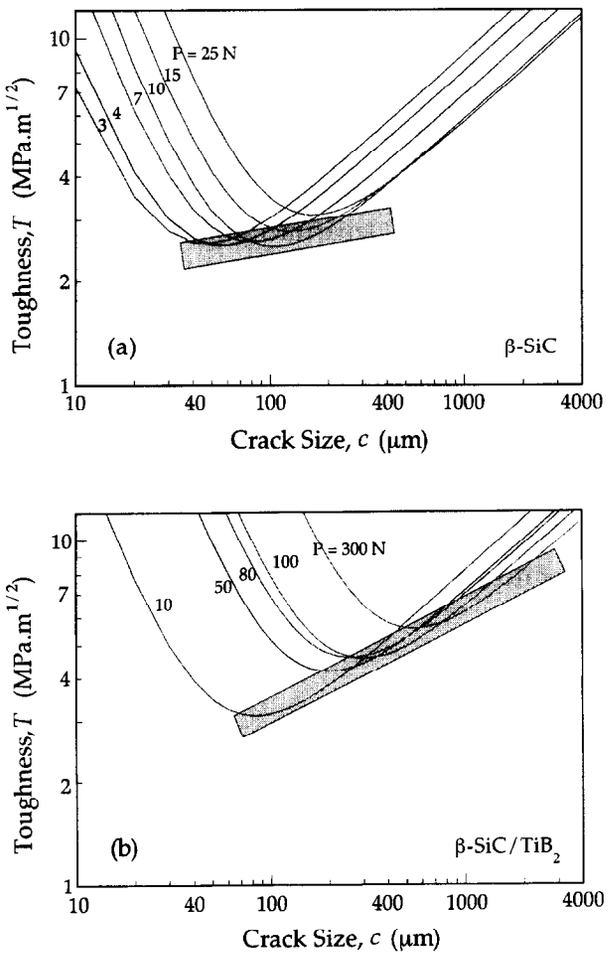

Fig. 6. Toughness-curve diagrams for (a) β-SiC and (b) β-SiC/TiB_2. The family of solid curves are plots of $K_A'(c)$ in eqn (1), using strength data from Fig. 4. Shaded bands are T-curves plotted as locus of tangency points to $K_A'(c)$ curves.

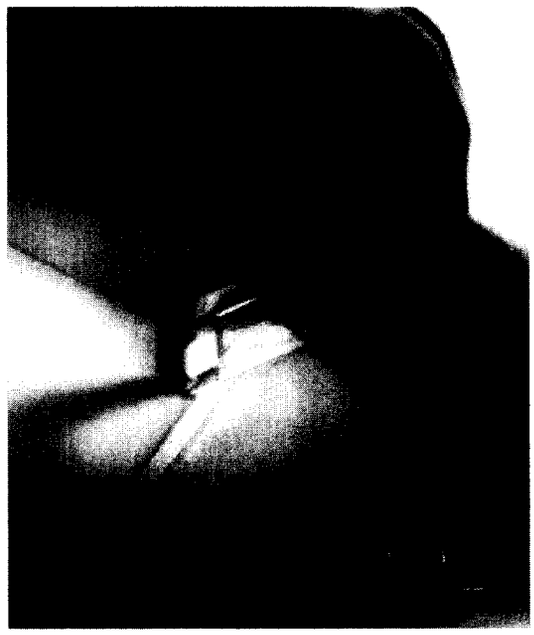

Fig. 7. TEM micrograph of a sintering aid granule at grain boundaries commonly found in α-SiC and α-SiC/TiB_2.

materials.[20] For crack bridging, the interface debonding between SiC and TiB_2 first needed to occur. The sources of a debonding interface were: (1) no chemical reactions between SiC and TiB_2 and (2) residual stresses at the interface. There was a thermal expansion mismatch between SiC ($\alpha = 5{\cdot}6\times10^{-6}\,K^{-1}$) and TiB_2 ($\alpha = 8{\cdot}5\times10^{-6}\,K^{-1}$), which caused residual stresses.[10] The residual tensile stress in the TiB_2 particulates enhanced debonding at the mterface. Although the interface debonding occurred, it was not weak enough to enable TiB_2 sliding and pullout easily which limited the toughening effect. This behavior was demonstrated by an arrow indicated in Fig. 2(a). The slightly strong interface between SiC and TiB_2 explained the increases in the strength and retained strength as TiB_2 was added to the matrix (Fig. 3). On the other hand, another toughening mechanism of stress-induced microcracking in α-SiC/TiB_2 has been proposed by Gu and Faber.[10,11]

Crack bridging also has been observed in Fig. 1(b) and 2(b) for β-SiC and its composite. Although crack deflection was observed, the rising $T(c)$ curve for β-SiC/TiB_2 could not be explained by a crack deflection model.[20] The residual stress effect between SiC and TiB_2, similar to α-type SiC materials, was a possible reason. The other contribution to interfacial debonding and a sharp T curve came from the intergranular phases in β-SiC and β-SiC/TiB_2. Amorphous silica between grains [Fig. 8(a)] and a crystalline aluminum silicate at a triple point [Fig. 8(b)] were observed and identified by EDS. The thermal expansion mismatch caused by these boundary phases also weakened the interface.

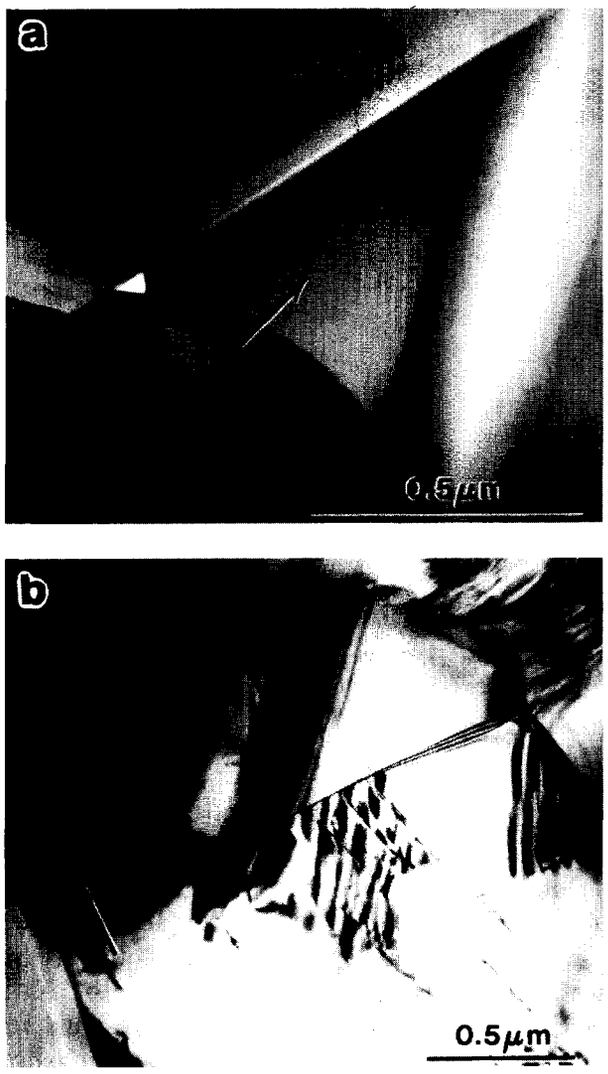

Fig. 8. TEM micrographs of interphases in Al_2O_3-sintered β-SiC and its composite, (a) amorphous silica phase and (b) crystalline aluminum silicate phase.

The stronger rising $T(c)$ curve for β-SiC/TiB_2, as compared with α-SiC/TiB_2, originated from the weak interface in the matrix and at SiC–TiB_2 interfaces. The behavior of the weak interfaces was shown in the strength degradation caused by adding TiB_2 to the SiC matrix (Fig. 4). The weak interface caused interfacial debonding, grain sliding, and grain pullout [Fig. 2(b)]. The sliding and pullout were the energy dissipating mechanisms and enhanced toughening. On the other hand, grain sliding and pullout were not easy for α-SiC/TiB_2, which gave less toughening. It has been shown that the crack resistance increases with crack extension and depends upon both the size and fraction of TiB_2 in α-SiC.[10] The size and fraction of TiB_2 in β-SiC were also important. The higher volume fraction of TiB_2 in β-SiC/TiB_2 provided a chance for toughening mechanisms to operate. The larger size of TiB_2 particulates in β-SiC/TiB_2 increased the crack closure forces[20–23] by TiB_2 bridging, sliding, and pullout, and thereby contributed to toughened β-SiC/TiB_2 with a sharp rising T curve.

5 Conclusions

In this study, we have shown that microstructure is crucial in controlling composite performance, by comparing two kinds of SiC and SiC/TiB_2 with indentation-strength tests and microstructural evaluations. T curves of these materials were analytically deconvoluted from the indentation-strength data. TiB_2 (15 vol%) in the boron- and carbon-doped α-SiC only increased the retained strength without a significant improvement in the toughening. On the other hand, TiB_2 (30 vol%) along with the effect of Al_2O_3 sintering aid for the β-SiC/TiB_2 composite greatly improved properties with a higher retained strength in long-crack regions, better flaw-tolerance behavior and a sharply rising T curve. The different toughening behaviors for α- and β-SiC/TiB_2 were related to the weak nature of the SiC–SiC and SiC–TiB_2 interfaces as well as the fraction and size of TiB_2.

Acknowledgements

The authors gratefully acknowledge valuable guidance from Dr Brian R. Lawn at NIST. This research was supported by the Federation of Advanced Manufacturing Industries (FAMI) affiliated with the Department of Materials Science and Engineering at UIUC. The authors would like to thank the Alcoa Company for manufacturing β-SiC and β-SiC/TiB_2 and the Carborundum Company for supplying the commercial Hexoloy α-SiC and α-SiC/TiB_2 specimens. The authors also wish to thank Dr Hongda Cai at Allied Signal Inc. for useful discussions. Use of the microstructure characterization facilities at the Center for Microanalysis of Materials in the Materials Research Laboratory at UIUC is acknowledged.

References

1. Li, C.-W. and Yamanis, J., Super-tough silicon nitride with R-curve behavior. *Ceram. Eng. Sci. Proc.*, 1989, **10**, 632–645.
2. Li, C.-W., Lee, D.-J. and Lui, S.-C., R-curve behavior and strength of *in-situ* reinforced silicon nitride with different microstructures. *J. Am. Ceram. Soc.*, 1992, **75**, 1777–1785.
3. Lee, S. K. and Kim, C. H., Effect of α-SiC versus β-SiC starting powders on microstructure and fracture toughness of SiC sintered with Al_2O_3–Y_2O_3 additives. *J. Am. Ceram. Soc.*, 1994, **77**, 1655–1658.
4. Lee, S. K., Kim, Y. C. and Kim, C. H., Microstructural development and mechanical properties of pressureless-sintered SiC with platelike grains using Al_2O_3–Y_2O_3 additives. *J. Mater. Sci.*, 1994, **29**, 5321–5326.

5. Padture, N. P., In situ-toughened silicon carbide. *J. Am. Ceram. Soc.*, 1994, **77**, 519–523.
6. Wei, G. C. and Becher, P. F., Improvements in mechanical properties in SiC by the addition of TiC particles. *J. Am. Ceram. Soc.*, 1984, **67**, 571–574.
7. Janney, M. A., Microstructural development and mechanical properties of SiC and of SiC–TiC composites. *Am. Ceram. Soc. Bull.*, 1986, **65**, 357–362.
8. McMurtry, C. H., Boecker, W. D. G., Seshadri, S. G., Zanghi, J. S. and Garnier, J. E., Microstructure and material properties of SiC–TiB_2 particulate composites. *Am. Ceram. Soc. Bull.*, 1987, **66**, 325–329.
9. Janney, M. A., Mechanical properties and oxidation behavior of a hot-pressed SiC–15 vol% TiB_2 composite. *Am. Ceram. Soc. Bull.*, 1987, **66**, 322–324.
10. Gu, W.-H., Faber, K. T. and Steinbrech, R. W., Microcracking and R-curve behavior in SiC–TiB_2 composites. *Acta Metall. Mater.*, 1992, **40**, 3121–3128.
11. Gu, W.-H. and Faber, K. T., Tensile behavior of microcracking SiC–TiB_2 composites. *J. Am. Ceram. Soc.*, 1995, **78**, 1507–1512.
12. Tani, T. and Wada, S., SiC matrix composites reinforced with internally synthesized TiB_2. *J. Mater. Sci.*, 1990, **25**, 157–160.
13. Viechnicki, D. J., Slavin, M. J. and Kliman, M. I., Development and current status of armor ceramics. *Am. Ceram. Soc. Bull.*, 1991, **70**, 1035–1039.
14. Padture, N. P. and Lawn, B. R., Toughness properties of a silicon carbide with an in situ induced heterogeneous grain structure. *J. Am. Ceram. Soc.*, 1994, **77**, 2518–2522.
15. Mai, Y.-W. and Lawn, B. R., Crack stability and toughness characteristics in brittle materials. *Ann. Rev. Mater. Sci.*, 1986, **16**, 415–439.
16. Lawn, B.R., *Fracture of Brittle Solids*, 2nd edn. Cambridge University Press, Cambridge, UK, 1993.
17. Marshall, D. B. and Lawn, B. R., Residual stress effect in sharp-contact cracking: 1. Indentation fracture mechanics. *J. Mater. Sci.*, 1979, **14**, 2001–2012.
18. Lawn, B. R., Evans, A. G. and Marshall, D. B., Elastic/plastic indentation damage in ceramics: the median/radial crack system. *J. Am. Ceram. Soc.*, 1980, **63**, 574–581.
19. Braun, L. M., Bennison, S. J. and Lawn, B. R., Objective evaluation of short-crack toughness curves using indentation flaws: case study on alumina-based ceramics. *J. Am. Ceram. Soc.*, 1992, **7**, 3049–3057.
20. Swanson, P. L., Fairbanks, C. J., Lawn, B. R., Mai, Y.-W. and Hockey, B. J., Crack-interface grain bridging as a fracture resistance mechanism in ceramics: 1. experimental study on alumina. *J. Am. Ceram. Soc.*, 1987, **70**, 279–289.
21. Lawn, B. R., Padture, N. P., Braun, L. M. and Bennison, S. J., Model for toughness-curves in two-phase ceramics: I, basic fracture mechanics. *J. Am. Ceram. Soc.*, 1993, **76**, 2235–2240.
22. Padture, N. P., Runyan, J. L., Bennison, S. J., Braun, L. M. and Lawn, B. R., Model for toughness-curves in two-phase ceramics: II, microstructural variables. *J. Am. Ceram. Soc.*, 1993, **76**, 2241–2247.
23. Cook, R. F., Fairbanks, C. J., Lawn, B. R. and Mai, Y.-W., Crack resistance by interfacial bridging: its role in determining strength characteristics. *J. Mater. Res.*, 1987, **2**, 345–356.